Structural and electrical properties of cerium dioxide films grown by RF magnetron sputtering

WEN-CHOU TSAI, TSEUNG-YUEN TSENG
Institute of Electronics and Department of Electronics Engineering, National Chiao-Tung University, Hsinchu, Taiwan

A systematic study was performed on the structural and electrical properties of cerium dioxide thin films grown on Si substrate with various deposition temperatures by RF magnetron sputtering. The films grown at 200 °C are partly amorphous whereas those grown above 250 °C are polycrystalline. An amorphous layer of SiO_2 forms at the interface between the cerium dioxide film and the Si substrate. Cerium dioxide film grown at higher temperatures up to 500 °C sustains more leakage current on the basis of current–voltage measurements. The electrical conduction of the films is well fitted by a power-law relation, which is explained as space-charge-limited current conduction with exponential distributed traps in the band gap. The variations of dielectric constant, flatband voltage, fixed oxide charge and interface-trapped charge with deposition temperature were studied by making capacitance–voltage measurements on an Al/CeO_2/Si structure. The variations of electrical properties with temperature are strongly correlated with the formation of an amorphous SiO_2 layer.

1. Introduction

Cerium dioxide has long been used in optical coating and polishing due to its transparency, chemical stability and hardness [1–3]. It shows an ionic conduction mechanism in its non-stoichiometric form and has attracted much investigation for use in gas sensors [4–7]. Due to its lattice match with high temperature superconductors, cerium dioxide has been widely adopted as the material of buffer layers or insulating layers for the growth of single-layer or multilayer epitaxial high temperature superconductor thin films [8–10]. It has also attracted renewed interest because of its potential application as a capacitor dielectric in dynamic random access memories (DRAMs) due to its relatively high dielectric constant of 26, compared with 3.9 for silicon dioxide [11–13].

We have explored the structural properties of epitaxial CeO_2 thin film grown on MgO and sapphire substrates [14]. However, the substrates are insulators and the electrical conduction is therefore limited. This study examines the structural and electrical properties of CeO_2 thin films grown on silicon substrates by RF magnetron sputtering.

2. Experimental procedure

CeO_2 thin films were deposited on p-type (1 1 1) silicon wafers with resistivity 4–7 Ω cm using RF magnetron sputtering in an argon plasma. The magnets of the sputter gun were arranged in an unbalanced figure with a weaker central magnet [15]. Compared with a balanced configuration, this magnet assembly appears to produce a smoother film surface and a higher deposition rate at low pressures. Details of the deposition setup are reported in the literature [14]. The target was a sintered CeO_2 disc of diameter 2 in. (51 mm). Before deposition the wafer was cleaned in aqueous H_2SO_4 to remove organic and metallic impurities, followed by an etch in dilute HF to remove the native silicon oxide.

Two sputtering conditions were used for the deposition of thin films: (A) chamber pressure 15 mtorr (2.0 Pa), pure argon ambient, 60 W RF power and various deposition temperatures; (B) same as condition A except the ambient was a mixture of argon and oxygen (flow rate ratios 3/1 and 30/1). The 60 W RF power yielded a growth rate of around 3 nm min^{-1}. The film thickness was around 100 nm. Al film was thermally evaporated on the deposited film as the gate of square-dot metal–insulator–semiconductor (MIS) capacitors with an area of 0.0013 cm^2. Contact on the backside of the Si wafer was obtained by depositing 1 μm thick Al film after etching off native SiO_2 with HF. The contacts were annealed in hydrogen at 450 °C for 30 min.

The deposited CeO_2 films had lower dielectric constant compared with bulk CeO_2. Thus we introduced oxygen into the chamber to change the deposition ambient, CeO_2 films grown under condition B can exhibit dielectric constants over 20. Hereafter, films grown under condition A are called A-films and films grown under condition B are called B-films.

0957–4522

Crystallinity of the grown films was examined by X-ray diffraction (XRD) and transmission electron microscopy (TEM). The film thickness was determined from cross-sectional TEM images. The refractive index of the film was measured by an ellipsometer using the 632.8 nm line of an He–Ne laser. The dielectric properties were studied by 1 MHz capacitance–voltage (*C–V*) measurement using the Keithley model-82 CV measuring system, and the leakage current by HP4145B.

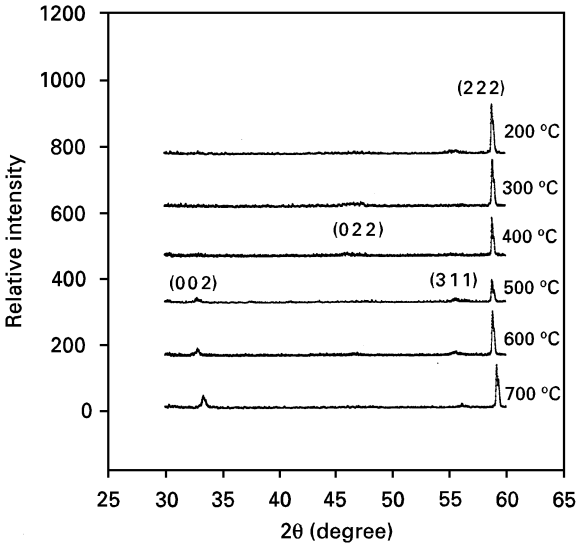

Figure 1 XRD spectra of A-films grown at various deposition temperatures.

3. Results and discussion

3.1. Structural properties

The structure of as-deposited films was examined as a function of deposition temperature. Fig. 1 shows XRD spectra of the A-films grown at various deposition temperatures. The A-films deposited at low temperatures ($< 300\,^{\circ}C$) are mainly (2 2 2) oriented and those deposited above 500 °C appear to have extra (0 0 2) and (3 1 1) diffraction peaks in their spectra. Generally speaking, the intensity of the (2 2 2) peak does not tend to decrease as the temperature is increased. The appearance of extra diffraction peaks indicates that the films grown at higher temperatures exhibit more random orientation. Yoshimoto *et al.* have shown that CeO_2 films grown on oxide-free (1 1 1) Si had (1 1 1) preferred orientation [16]. In this study the as-deposited films were polycrystalline and had (2 2 2) preferred orientation, like those reported previously. The minor grains with other orientations on the film are ascribed to grown SiO_2. It is well known that a fresh Si surface would be easily covered by silicon oxide on exposure to the air. This as-grown amorphous SiO_2 generally inhibits the epitaxial growth of any following layer.

Fig. 2 shows TEM electron diffraction patterns of the A-films grown at various deposition temperatures. The film deposited at 200 °C shows the coexistence of amorphous halo diffraction and obscure polycrystalline rings. The film deposited at 250 °C is crystallized (Fig. 2b) and those grown at a temperature of 500 °C or higher are polycrystalline (Fig. 2c). Overlap of Si diffraction spots on the polycrystalline rings reveals that the films exhibit an exact fluorite structure because CeO_2 is lattice-matched with Si.

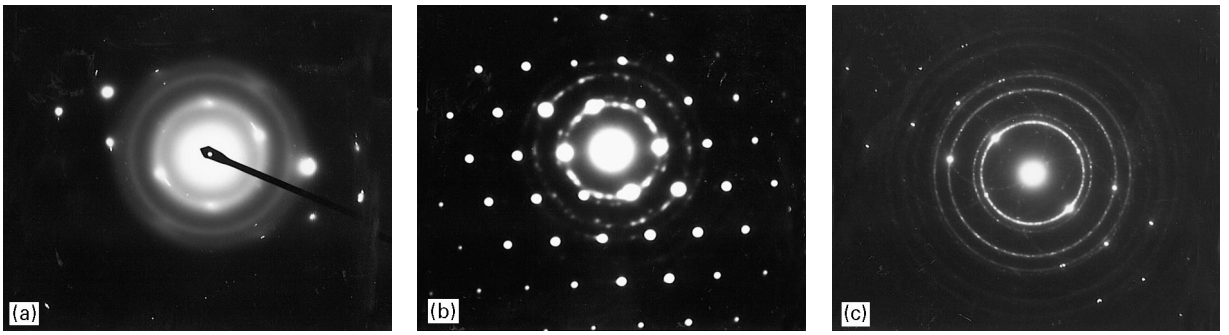

Figure 2 TEM electron diffraction patterns of A-films deposited at (a) 200 °C, (b) 250 °C and (c) 500 °C.

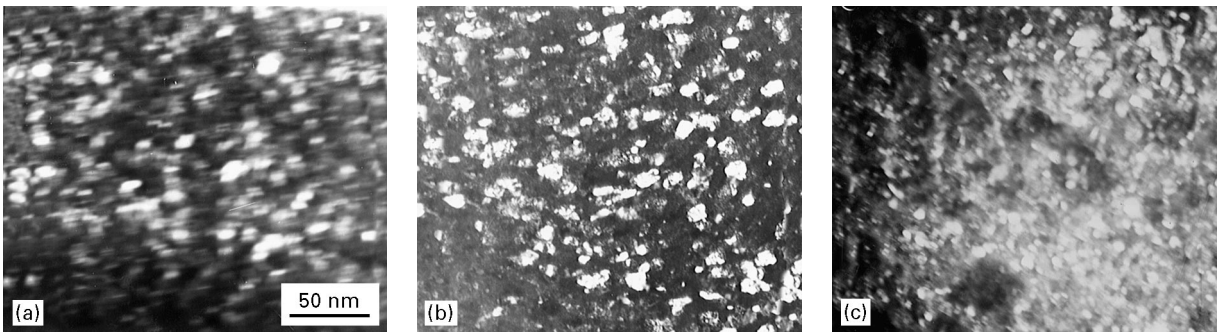

Figure 3 TEM dark-field images of A-films deposited at (a) 250 °C, (b) 400 °C and (c) 700 °C.

Fig. 3 shows TEM dark-field images on (0 0 2) rings of the A-films grown at 250 °C, 400 °C and 700 °C, respectively. Although XRD spectra of the A-films grown at higher temperatures show stronger polycrystallinity, the sizes of (0 0 2) oriented grains on TEM images do not become larger as the deposition temperature increases. Calculations based on XRD peak broadening indicate the grain size in the film is about 26 nm, consistent with Fig. 3.

Fig. 4 shows the cross-sectional TEM images of the A-films deposited at 300 °C and 700 °C. Notice the amorphous SiO_2 layer underneath the as-deposited film. This was generally observed during deposition or post-annealing of oxide film on Si [17, 18]. The variation of SiO_2 thickness with deposition temperature is illustrated in Fig. 5. The SiO_2 thickness is around 2.6–3.6 nm up to a deposition temperature of 600 °C. Compared to the 100 nm thick CeO_2 film, the SiO_2 layer with thickness less than 4.0 nm is thin, which is not considered an effective insulator if an electric field is applied across the MIS capacitor. The fresh Si wafer is considered to grow SiO_2 of no more than 1.0 nm in thickness before thin film growth based on the results of Fenner *et al.* [19]. All SiO_2 layers in our study are thicker than 1.0 nm, so additional SiO_2 grows during the deposition of CeO_2 films. Fig. 4 indicates that the SiO_2–Si interface is atomically sharp and clear but the CeO_2–SiO_2 interface is somehow not as clear. The CeO_2–SiO_2 interface is even more ambiguous; this is because the A-film grows at higher temperature (Fig. 4b). The ambiguous interface may be attributed to the increased interdiffusion between CeO_2 and Si.

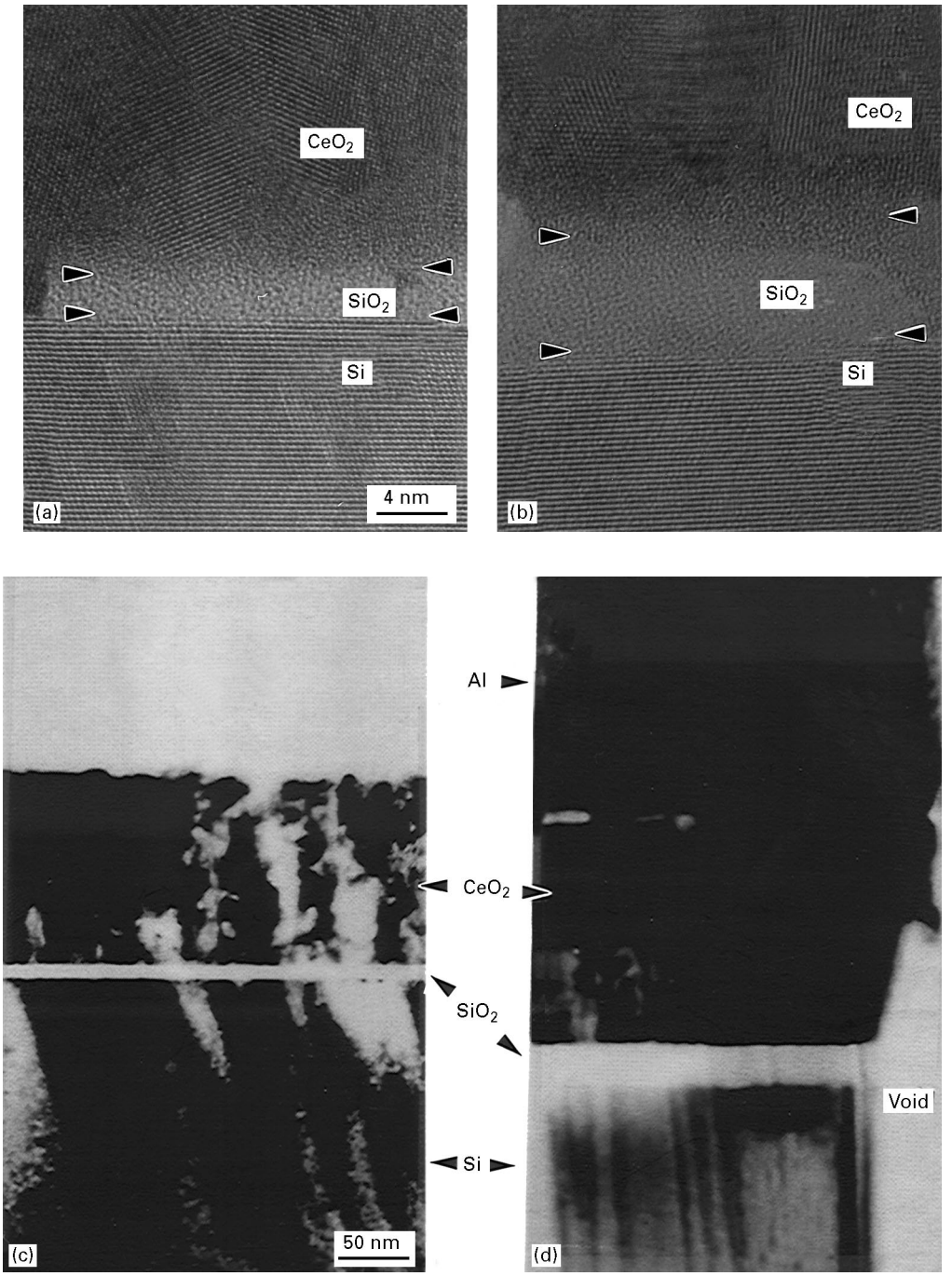

Figure 4 Cross-sectional TEM images for A-films deposited at (a) 300 °C (b) 700 °C and for B-films deposited at (c) 500 °C and (d) 700 °C. An amorphous SiO_2 layer is formed between the film and the Si substrate.

Fig. 6 shows that the B-films grown at 500 °C and 700 °C also reveal (2 2 2) dominant diffraction in their XRD spectra and other diffraction peaks, e.g. (0 0 2), (3 1 1) and (0 2 2), are not greatly enhanced compared with Fig. 1. Therefore, the introduction of oxygen during deposition does not change the crystal orientation of as-grown B-films. One feature of the grown B-films is a drastic thickness increase of the SiO_2 layers compared with the A-films (Fig. 4c and d). SiO_2 layers with thicknesses of 11.0 nm and 32.0 nm are observed beneath the B-films.

3.2. Refractive index

Variation of the refractive index with deposition temperature is shown in Fig. 5. The refractive index of CeO_2 is not affected by the interfacial SiO_2 layer, which is too thin compared with the thickness of CeO_2 film deposited up to 600 °C. The refractive index approximately follows a monotone increase with deposition temperatures lower than 500 °C, remains at 2.46 in the range 500–650 °C and has fallen to below 2.38 at a deposition temperature of 700 °C. The refractive index of the thin film depended significantly on the measuring wavelength [2, 3]. It might also have been influenced by any change in the film crystallinity, the refractive index of the films presumably improved with a higher degree of structural ordering [20]. However, only a small change in the refractive index was observed within the deposition temperature range, from 2.32 at 250 °C to 2.46 at 500 °C. XRD spectra reveal more diffraction peaks for films grown at higher deposition temperature (Fig. 1). Thus the small increase in the refractive index of A-films with increasing deposition temperature seems to be related to the polycrystallinity of the films. The slight decrease of the refractive index at 700 °C can be ascribed to the thickened SiO_2 layer, as shown in Fig. 5.

3.3. Current–voltage characteristics

The leakage current was measured by the change of negative bias on the top Al electrode such that p-type Si substrate was in accumulation and there was electron injection from the Al gate into the CeO_2. The leakage current density in those as-deposited films is generally high and it tends to increase with increasing deposition temperature, as shown in Table I. The lower leakage current of the A films grown at above 600 °C can be ascribed to the thickened SiO_2 layer, as

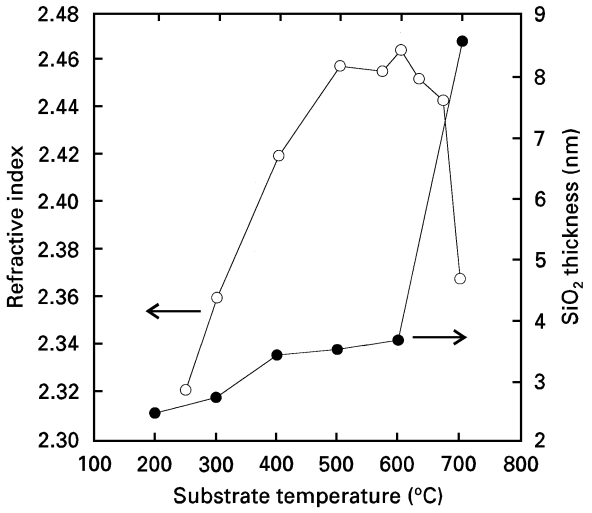

Figure 5 (●)Thickness of the SiO_2 layer and (○) refractive index of A-films as a function of deposition temperature.

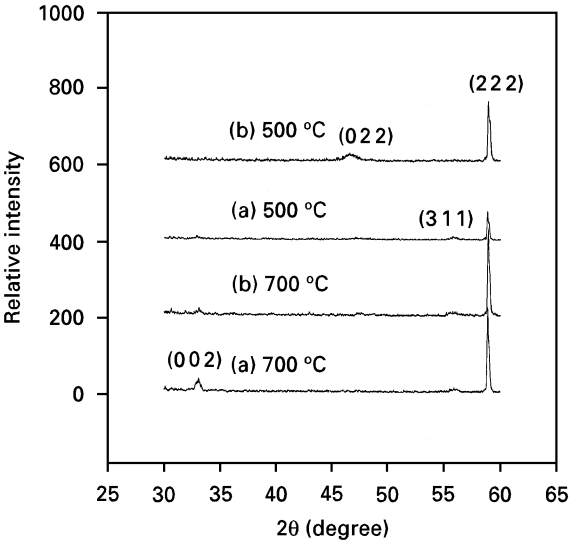

Figure 6 XRD spectra of B-films deposited with argon/oxygen flow rates in the ratios (a) 30/1 and (b) 3/1.

TABLE I Dielectric constant (ε_r), flatband voltage (V_{FB}), density of fixed oxide charge (N_f), density of interface trapped charge (D_{it}), flatband voltage shift (ΔV_{FB}) (evaluated from C–V curves) and leakage current density (at 0.4 MV cm^{-1}) for A-films and B-films prepared at various deposition temperatures

Growth condition	ε_r	V_{FB} (V)	N_f (cm^{-2})	D_{it} (eV^{-1} cm^{-2})	ΔV_{FB} (V)	J (A cm^{-2})
A, 700 °C	8.32	− 3.25	1.15×10^{12}	3.3×10^{12}	0.12	1.3×10^{-8}
A, 600 °C	7.2	− 2.39	0.37×10^{12}	0.72×10^{12}	0.30	6.0×10^{-7}
A, 500 °C	7.7	− 1.55	0.22×10^{12}	0.29×10^{12}	1.18	1.1×10^{-6}
A, 400 °C	6.9	− 1.54	0.19×10^{12}	0.27×10^{12}	1.34	4.6×10^{-7}
A, 300 °C	4.7	− 1.43	0.17×10^{12}	0.22×10^{12}	1.92	1.1×10^{-7}
A, 200 °C	5.9	− 1.38	0.15×10^{12}	1.22×10^{12}	3.50	3.8×10^{-8}
B, 500 °C, 30/1[a]	22.9	− 7.5	3.72×10^{12}	2.55×10^{12}	0.28	2.0×10^{-7}
B, 500 °C, 3/1[a]	22.8	− 7.9	5.03×10^{12}	8.98×10^{12}	0.23	2.3×10^{-8}
B, 700 °C, 30/1[a]	18.8	− 2.98	1.29×10^{12}	16.0×10^{12}	0.37	2.5×10^{-8}
B, 700 °C, 3/1[a]	24.6	− 3.55	1.32×10^{12}	7.99×10^{12}	0.12	2.3×10^{-8}

[a] Argon/oxygen flow rate ratio.

shown in Fig. 5. A good insulator, the SiO_2 layer compensates for the relatively high leakage current of many high dielectric constant MIS gate oxides such as Ta_2O_5 and Y_2O_3 [21, 22]. Since the formation of SiO_2 on silicon is generally observed in a conventional sputter system, thickness control of the SiO_2 layer is important to maintain the overall dielectric constant above a suitable high value. Fig. 7 shows an Arrhenius plot of current through an MIS diode with CeO_2 gate oxide (A-film) grown at 500 °C. The current density (J_S) is independent of the measurement temperature below 200 K; this implies tunnelling or field emission conduction for current transport through the oxide. The current density follows an exponential relationship with measurement temperature above 200 K, $J_S \propto \exp(-E_a/kT)$, where $E_a = 0.32$ eV is the activation energy estimated from the data. This value agrees with those reported by others, confirming electrons as the charge carriers through CeO_2 [4, 7].

Fig. 8 shows both the negative and positive biased I–V characteristics for the A-films deposited at 500 °C. The I–V curves at low applied voltage show an ohmic-like characteristic. The positive bias current saturates above 16 V and the negative bias current does not saturate at the highest applied voltage of 20 V (corresponding to 2 MV cm^{-1}). All the films show rapidly increasing leakage current at applied negative voltages of around 5–10 V followed by more slowly increasing leakage current at voltages above 10 V. Fig. 9 takes the I–V curves of Fig. 8 and replots them using lnV as the horizontal axis. The best fit to the curve is a power-law relation, $I \propto V^{+\eta}$ where $\eta = 6$.

Among the commoner basic electrical conduction mechanisms, the only one that appears to match this empirical formula is space-charge-limited current (SCLC) conduction [23, 24]. The space charge is built up when the rate of carrier injection from the contact exceeds the rate at which the carriers can be transported across the film. For SCLC conduction to occur, at least one contact must be ohmic. Thus Ohm's law is obeyed at very low densities of the injected carrier, but the relationship between current and voltage is non-linear at higher field and the SCLC conduction follows a square law, $I \propto V^2$. The I–V curve transfers from ohmic conduction to SCLC conduction at a transfer voltage (V_t) as shown in Fig. 9. However, if many sets of traps are distributed throughout the energy gap of the oxide, the injected carriers are removed by empty traps, so the SCLC is reduced.

Mark and Helfrich have shown that SCLC conduction limited by exponentially distributed traps satisfies the I–V relation $I \propto V^{n+1}$ where $n = T_c/T$ and T_c is the characteristic temperature of the trap distribution [25]. The transfer voltage V_t is given by $V_t = qkT_cN_nd^2/\varepsilon$, where d is the oxide thickness [26]. Thus in a space charge region with an exponential distribution of traps, the transfer voltage should vary with the square of d. In this study a distribution of trap levels is expected because a large amount of structural disorders exists in the polycrystalline film, as shown in

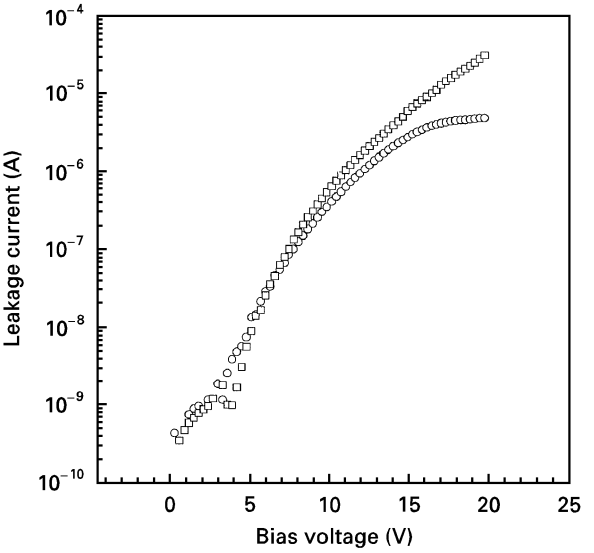

Figure 8 I–V curves with (□) negative and (○) positive bias voltages for A-films deposited at 300 °C.

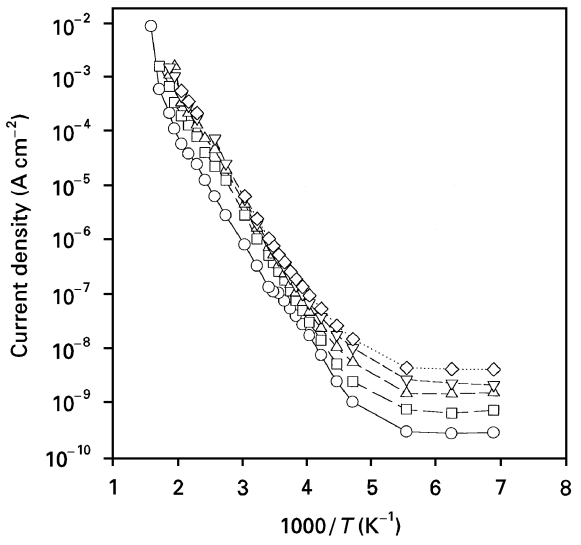

Figure 7 Leakage current as a function of inverse temperature and bias voltage for A-films deposited at 500 °C: (○) bias voltage = 2 V, (□) 4 V, (△) 6 V, (▽) 8 V, (◇) 10 V.

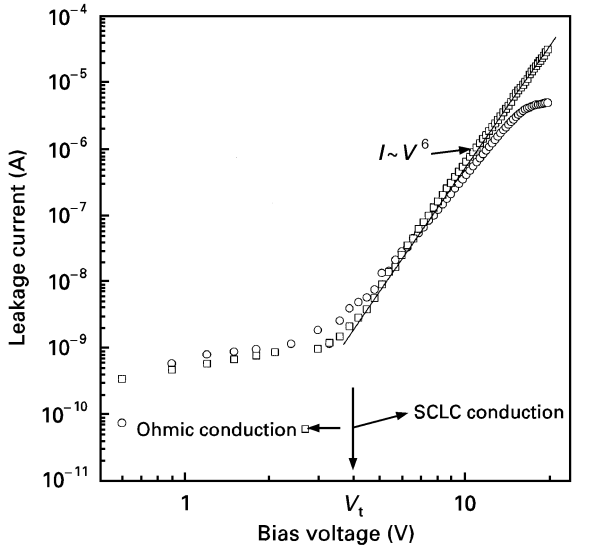

Figure 9 The I–V curves of Fig. 8 replotted using ln V as the horizontal axis: (□) negative bias and (○) positive bias.

Fig. 4, and it is reasonable to assume the I–V curve will not follow the simple square law. Fig. 10 shows that the transfer voltage varies linearly with the square of the A-film thickness up to 0.2 μm. The results are consistent with SCLC conduction behaviour. Thus, it is concluded that I–V curves obey ohmic conduction at low voltages (<5 V) and exhibit SCLC conduction at high voltages (>5 V) as $\eta = 6$. At even higher applied voltages (>16 V) , the current reaches saturation for a positive bias voltage. This saturation arises from the limited number of electrons supplied by the p-Si to the insulator.

Current–voltage curves of B-films exhibit SCLC conduction similar to that for A-films (the curves are omitted for brevity). The leakage current for B-films is generally lower than for A-films, presumably due to the thicker SiO_2 layers beneath the B-films. The only exception is the film deposited at 700 °C, which is yet to be explained.

3.4. Capacitance–voltage characteristics

The results of C–V measurements show that all the films exhibit typical MIS behaviour where regions of accumulation, depletion and inversion are present. Oxide capacitance of the films, i.e. MIS capacitance in accumulation, increases slightly with increasing deposition temperature. Table I lists related dielectric constants of the films calculated from the C–V measurements. The dielectric constants of CeO_2 films given in Table I were obtained by deleting a serial SiO_2 capacitor having a lower dielectric constant of 3.9. The variation of dielectric constant for A-films is similar to the change in refractive index (Fig. 5). The highest dielectric constant obtained for the A-films deposited at 500 °C is lower than the value for bulk CeO_2. Introduction of oxygen during deposition dramatically improves the dielectric constant of the grown films; the highest dielectric constant of B-films approaches the value of bulk CeO_2.

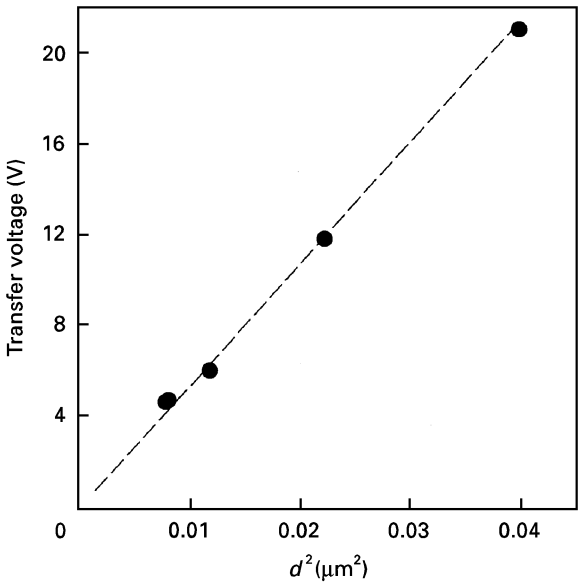

Figure 10 Transfer voltage as a function of the squared film thickness.

The flatband voltage V_{FB} corresponds to the flatband capacitance (C_{FB}) on the C–V curve; V_{FB} exhibits a negative shift with increased deposition temperatures for A-films, as shown in Table I. This indicates that positive oxide charges in the A-films increase with increasing deposition temperature. The crystallinity of the A-film is improved by increasing the deposition temperature, so an increase of oxide charge in CeO_2 films is not expected. Therefore, we relate the change of V_{FB} to a thickness change of the interfacial amorphous SiO_2 layer with increasing deposition temperature. It appears the oxide charges dominating V_{FB} are mainly contributed by the amorphous SiO_2 layer. V_{FB} is readily related to the fixed oxide charge density (N_f) by the relation $V_{FB} = \phi_{ms} - qN_f/C_0$, where ϕ_{ms} is the work function difference between the Al gate and silicon and C_0 is the oxide capacitance in accumulation [27]. As shown in Table I, N_f increases with increasing deposition temperatures for the A-films. Thin film deposited at 200 °C with amorphous phase in the majority does not have higher N_f.

It has been reported that SiO_2 layers grown on Si at higher deposition temperatures exhibit lower N_f [28]. Our B-films are consistent with this tendency, perhaps due to a thicker SiO_2 layer, but our A-films appear to differ. Since N_f is obtained from V_{FB}, which relates to properties of the SiO_2 layer, the different tendency in N_f varied with increasing deposition temperature and may be attributed to the different properties of the SiO_2 layer grown under the two different conditions, A and B. It is probable that N_f in SiO_2 is increased by the enhanced interdiffusion between CeO_2 and SiO_2 at high deposition temperatures. Note that N_f for the B-films is apparently larger than for the A-films, as shown in Table I, due to the introduction of oxygen during sputtering. Similar results have been clearly observed for thermally grown SiO_2 on Si [27, p. 245], thus it is reasonable to suggest that interfacial SiO_2 dominates the variation of V_{FB} and N_f in our films.

At the flatband voltage, the interface-trapped charge density D_{it} is given by

$$D_{it} = (C_0 - C_{FB})\ C_{FB}[3qkTA(\mathrm{d}C/\mathrm{d}V)]^{-1} - C_0^2[Aq^2(C_0 - C_{FB})]^{-1}$$

where $\mathrm{d}C/\mathrm{d}V$ is the slope at V_{FB}, and A is the electrode area. D_{it} at V_{FB} is listed in Table I. It is found that for A-films an increase in deposition temperature leads to higher D_{it}, like N_f. It has been observed in RF sputtered strontium titanate thin films on Si that an increasing D_{it} depends on the promoted formation of an interfacial SiO_2 layer during the deposition [29]. The existence of an SiO_2 layer would increase defect densities along with trapping centres and surface states at the interface regions. The A-film deposited at 200 °C somehow shows a remarkably higher D_{it} than the others deposited at the higher temperatures, except 700 °C. This high D_{it} might be ascribed to the crystallinity of the film because the film deposited at 200 °C is partly amorphous.

Fig. 11 shows 1 MHz C–V plots for MIS capacitors with gate oxides (A-film) deposited at 700 °C in which

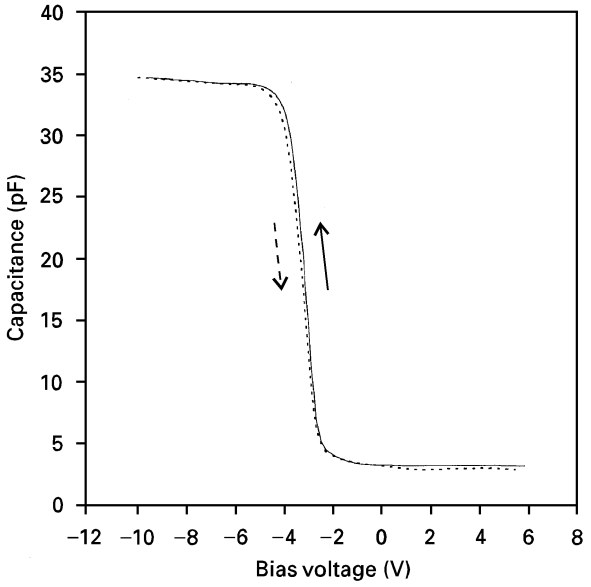

Figure 11 Hysteresis in the 1 MHz C–V behaviour of the Al–CeO_2–p-Si MIS structure for A-films grown at 700 °C.

the voltage is swept continuously as the arrows indicate. Films on p-type silicon show a carrier-injection-type hysteresis (counterclockwise rotation), where charges are injected from the silicon surface to trapping centres in the deposited film. A higher defect concentration in the film of lower crystallization is expected to create a large number of trapping centres, which may accommodate more electrons (trapped charge) injected from the electrode, causing a greater shift of the flatband voltage (ΔV_{FB}) in hysteresis curves of C–V measurements. Table I shows that ΔV_{FB} is more relevant for A-films deposited at lower temperatures. A-films deposited at higher temperatures seem to exhibit lower amounts of trapped charge injected into the films during the bias cycle. This implies better crystallinity in the films grown at higher temperatures. B-films have lower ΔV_{FB} than most A-films as illustrated in Table I. This can be ascribed to their better crystallinity (higher dielectric constant) and their thick SiO_2 layer [30].

Although the dielectric constant of CeO_2 films can be increased to over 20 by introducing oxygen into the plasma, this does cause the formation of thick SiO_2 layers, which lower the overall dielectric constant of CeO_2–SiO_2 composite layers. The dielectric constant for B-films including SiO_2 layers is around 17. This lowering of the dielectric constant is unfavourable for DRAM capacitors. Methods to grow CeO_2 films with high dielectric constant, while suppressing SiO_2 growth are therefore expected. A high oxygen diffusion resistance bottom electrode on Si is more feasible for growing high dielectric constant CeO_2 films with thin SiO_2 layers. On the other hand, perhaps due to the polycrystallinity of the films, the leakage current of our CeO_2 films is two orders of magnitude higher than for epitaxial CeO_2 films grown by Tye *et al.* [31]. However, with respect to their application in gigabit DRAM dielectrics, a leakage current density of less than 1×10^{-7} A cm^{-2} at 1 V is required [32], thus our films are quite satisfactory.

4. Summary

CeO_2 film deposited by RF magnetron sputtering above 250 °C is polycrystalline whereas film deposited below 200 °C is partly amorphous. An amorphous SiO_2 layer is observed between CeO_2 film and silicon. When the film is grown without oxygen flow and at higher temperatures, the dielectric constant increases up to 500 °C, but it remains as low as 6–8 in comparison with 26 for bulk CeO_2. When the film is grown under oxygen flow, its dielectric constant can be drastically improved to over 20. Results of C–V measurements show that the densities of interface-trapped charge and fixed oxide charge in the films increase with increasing deposition temperature. These two charge densities appear to be dominated by the as-grown SiO_2 layer. I–V measurements indicate that the electrical conduction is well fitted by a power-law relation; this can be explained by SCLC conduction with distributed traps in the energy gap of the oxide.

Acknowledgement

The authors gratefully acknowledge financial support from the National Science Council of China under contract NSC 85-2112-M009-037.

References

1. W. J. COLEMAN, *Appl. Opt.* **13** (1974) 946.
2. R. P. NETTERFIELD, W. G. SAINTY, P. J. MARTIN and S. H. SIE, *ibid.* **24** (1985) 2267.
3. K. B. SUNDARAM, P. F. WAHID and P. J. SISK, *Thin Solid Films* **221** (1992) 13.
4. G. BOUREAU, O. MASMOUDI and R. TETOT, *Solid State Commun.* **79** (1991) 299.
5. H. L. TULLER and A. S. NOWICK, *J. Electrochem. Soc.* **126** (1979) 209.
6. A. MARTINEZ-ARIAS, J. SORIA, J. C. CONESA, X. L. SEOANE, A. ARCOYA and R. CATALUÑA, *J. Chem. Soc. Faraday Trans.* **91** (1995) 1679.
7. H.-J. BEIE and A. GNÖRICH, *Sensors and Actuators* **B4** (1991) 393.
8. M. W. DENHOFF and J. P. McCAFFREY, *J. Appl. Phys.* **70** (1991) 3986.
9. S. S. LEE and D. YOUM, *Physica C* **211** (1993) 205.
10. W. L. HOLSTEIN, L. A. PARISI, D. W. FACE, X. D. WU, S. R. FOLTYN and R. E. MUENCHAUSEN, *Appl. Phys. Lett.* **61** (1992) 982.
11. T. NAKAZAWA, T. INOUE, M. SATOH and Y. YAMAMOTO, *Jpn. J. Appl. Phys.* **34** (1995) 548.
12. T. HIRAI, K. TERAMOTO, K. NAGASHIMA, H. KOIKE and Y. TARUI, *ibid.* **34** (1995) 4163.
13. A. G. FRANGOUL, K. B. SUNDARAM and P. F. WAHID, *J. Vac. Sci. Technol. B* **9** (1991) 181.
14. W. C. TSAIH, C. K. HUANG and T. Y. TSENG, *J. Amer. Ceram. Soc.* **78** (1995) 1969.
15. B. WINDOW and N. SAVVIDES, *J. Vac. Sci. Technol. A* **4** (1986) 196.
16. M. YOSHIMOTO, H. NAGATA, T. TSUKAHARA and H. KOINUMA, *Jpn. J. Appl. Phys.* **29** (1990) L1199.
17. T. CHIKYOW, S. M. BEDAIR, L. TYE and N. A. EL-MASRY, *Appl. Phys. Lett.* **65** (1994) 1030.
18. T. INOUE, T. OHSUNA, Y. OBARA, Y. YAMAMOTO, M. SATOH and Y. SAKURAI, *Jpn. J. Appl. Phys.* **32** (1993) 1765.
19. D. B. FENNER, D. K. BIEGELSEN and R. D. BRINGANS, *J. Appl. Phys.* **66** (1989) 419.
20. D. A. CHANG, P. LIN and T. Y. TSENG, *J. Appl. Phys.* **78** (1995) 7103.

21. S. BANERJEE, B. SHEN, I. CHEN, J. BOHLMAN, G. BROWN and R. DOERING, *J. Appl. Phys.* **65** (1989) 1140.
22. A. C. RASTOGI and R. N. SHARMA, *J. Appl. Phys.* **71** (1992) 5041.
23. S. M. SZE, "Physics of Semiconductor Devices" (Wiley, New York, 1981) p. 403.
24. A. ROSE, *Phys. Rev.* **97** (1955) 1538.
25. P. MARK and W. HELFRICH, *J. Appl. Phys.* **33** (1962) 205.
26. J. G. SIMMONS, in "Handbook of Thin Film Technology", edited by L. I. Maissel and R. Glang (McGraw-Hill, New York, 1970), p. 14.
27. D. K. SCHRODER, "Semiconductor Material and Device Characterization" (Wiley, New York, 1990) p. 225.
28. E. H. SNOW, *J. Electrochem. Soc.* **114** (1967) 266.
29. J. R. BELSICK and S. B. KRUPANIDHI, *J. Appl. Phys.* **74** (1993) 6851.
30. K. LEHOVEC, *Solid-state Elec.* **11** (1968) 135.
31. L. TYE, N. A. EL-MASRY, T. CHIKYOW, P. MCLARTY and S. M. BEDAIR, *Appl. Phys. Lett.* **65** (1994) 3081.
32. T. Y. TSENG, *IEDMS*, **C2-5** (1996) 89.

Received 11 October 1996
and accepted 10 January 1997